

AC Magnetic Field Sensing Using Continuous-Wave Optically Detected Magnetic Resonance of Nitrogen Vacancy Centers in Diamond

Soya Saijo,¹ Yuichiro Matsuzaki,² Shiro Saito,² Ikuya Hanano,¹ Hideyuki Watanabe,³ Norikazu Mizuochi,⁴ and Junko Ishi-Hayase¹

¹*Faculty of Science and Technology, Keio University, Hiyoshi, Kohoku-ku, Yokohama 223-8522, Japan*

²*NTT Basic Research Laboratories, NTT Corporation, 3-1 Morinosato-Wakamiya, Atsugi, Kanagawa, 243-0198, Japan.*

³*Correlated Electronics Group, Electronics and Photonics Research Institute, National Institute of Advanced Industrial Science and Technology, Higashi, Tsukuba, Ibaraki 305-8565, Japan*

⁴*Institute for Chemical Research, Kyoto University, Gokasho, Uji-city, Kyoto 611-0011, Japan*

Nitrogen-vacancy (NV) centers in diamond are considered sensors for detecting magnetic fields. Pulsed optically detected magnetic resonance (ODMR) is typically used to detect AC magnetic fields; however, this technique can only be implemented after careful calibration that involves aligning an external static magnetic field, measuring continuous-wave (CW) ODMR, determining the Rabi frequency, and setting the microwave phase. In contrast, CW-ODMR can be simply implemented by continuous application of green CW laser and a microwave field. In this letter, we report a method that uses NV centers and CW-ODMR to detect AC magnetic fields. Unlike conventional methods that use NV centers to detect AC magnetic fields, the proposed method requires neither a pulse sequence nor an externally applied DC magnetic field; this greatly simplifies the procedure and apparatus needed to implement this method. This method provides a sensitivity of $2.5 \mu\text{T}/\sqrt{\text{Hz}}$ at room temperature. Thus, this simple alternative to existing AC magnetic field sensors paves the way for a practical and feasible quantum sensor.

Nitrogen-vacancy (NV) centers in diamond can be used as sensitive room temperature magnetic field sensors with submicron spatial resolution¹⁻³. Many variations of NV center magnetic field sensors exist, such as vector magnetic field sensing via confocal microscopy^{4,5}, rapid imaging using charge coupled device (CCD) arrays⁶⁻¹⁰, and atomic force microscopy, which provides nanoscale imaging using a nanodiamond or a diamond nanopillar tip¹¹⁻¹⁵.

To demonstrate a magnetic field sensor, either a pulsed ODMR technique or CW-ODMR technique may be used. The pulsed ODMR technique has been applied to detect both AC and DC magnetic fields^{3,16,17}. Although the pulsed ODMR technique provides better sensitivity than the CW-ODMR technique, it requires careful calibration before it can detect a magnetic field. This calibration typically involves aligning an external static magnetic field, measuring CW-ODMR, observing Rabi oscillations (to determine the Rabi frequency), controlling the microwave phase, and constructing a pulse sequence. Pulsed ODMR detects high frequency magnetic fields by narrowing the pulse interval, which is technically possible, but this method is not easy from the viewpoint of the coherence time of NV center and the cost of the high speed control device.

In contrast, the CW-ODMR technique can be used to detect DC magnetic fields or low frequency (e.g., kHz) AC magnetic fields, and it is a more convenient technique because it only requires the continuous application of microwaves and an optical laser. Although the sensitivity of CW-ODMR is currently lesser than that of the pulsed ODMR, its simple experimental requirements have led many researchers to use it for practical and feasible magnetic field measurements.

To extend the applications of CW-ODMR method, using

CW-ODMR with NV centers in diamond, we developed a method to measure AC magnetic fields up to MHz frequencies. Already, the CW-ODMR method is being used to measure AC magnetic fields in the kHz frequency range; in this technique, magnetic fields are applied to exploit the two level nature of NV centers¹⁸⁻²⁰. In contrast, in the present work, we use the spin-1 properties of NV centers to measure AC magnetic fields with MHz frequencies. Three energy eigenstates exist in the ground state manifold of NV centers, all of which are used for magnetic field sensing. The lowest energy eigenstate $|0\rangle$ is about 2.87 GHz below the two higher energy eigenstates, which themselves have an energy difference in the order of MHz. The idea behind the proposed method is to use this MHz transition frequency to detect AC magnetic fields while the lowest energy eigenstate is continuously excited by the continuous microwave radiation.

Note that the CW-ODMR technique is compatible with CCD based techniques that have slow camera frame rate. Since CCD cameras detect a wide field, the magnetic field information in diamond may be collected over a wide area in a single measurement. This allows the magnetic field distribution to be rapidly acquired because, unlike other techniques, the magnetic field in diamond does not need to be measured point by point. However, a potential problem of the CCD based scheme is the slow camera operation time (from 100 Hz to 1 kHz). Since the pulse repetition rate exceeds a few MHz for typical AC magnetic field sensing, sophisticated techniques such as the use of optical shutters are required^{6,9}. Conversely, because the CW-ODMR technique does not invoke such fast operations, in our AC magnetic field sensors provides a way to adopt the CCD based technique with much more simple experimental setup. Since the CCD based setup can increase the measurement volume of NV centers,

the signal from the NV is enhanced and highly sensitive sensing becomes possible. Furthermore, no external static magnetic field is used, the measurement volume can be increased without concern for the uniformity of the static magnetic field.

We start by explaining the theory behind both the conventional methods and the proposed method. The Hamiltonian of an NV center with no external magnetic field is given as follows.

$$H_{\text{NV}} = D\hat{S}_z^2 + E_x(\hat{S}_x^2 - \hat{S}_y^2) + E_y(\hat{S}_x\hat{S}_y - \hat{S}_y\hat{S}_x) \quad (1)$$

where \hat{S} is a spin-1 operator for electron spin, D is the zero field splitting, and $E_x(E_y)$ is the strain in the $x(y)$ direction. Without loss of generality, we set $E_y = 0$ by defining the x axis to pass through the NV center in the direction of the strain. Throughout this letter, we set $\hbar = 1$. The ground state is $|0\rangle$, and we define the two higher energy eigenstates as $|D\rangle = (|1\rangle - |-1\rangle)/\sqrt{2}$ and $|B\rangle = (|1\rangle + |-1\rangle)/\sqrt{2}$ with eigenenergies $D - E_x$ and $D + E_x$, respectively. With zero external magnetic field, two dips appear around 2.87 GHz in CW-ODMR, which is indicative of externally driven transitions from the ground state $|0\rangle$ to higher energy eigenstates such as $|B\rangle$ or $|D\rangle$ ²¹⁻²³.

We now consider the dynamics of NV centers when both the microwave field and the target AC magnetic field are present. With these external fields, the Hamiltonian of the NV center takes the form $H = H_{\text{NV}} + H_{\text{ex}}$, where H_{ex} is given by

$$H_{\text{ex}} = \sum_{j=x,y,z} \gamma_e B_{\text{mw}}^{(j)} \hat{S}_j \cos(\omega_{\text{mw}} t) + \gamma_e B_{\text{AC}}^{(j)} \hat{S}_j \cos(\omega_{\text{AC}} t) \quad (2)$$

where γ_e is the gyromagnetic ratio of the electron spin, $B_{\text{mw}}(B_{\text{AC}})$ is the microwave field (target AC magnetic field) amplitude, and $\omega_{\text{mw}}(\omega_{\text{AC}})$ is the frequency of the

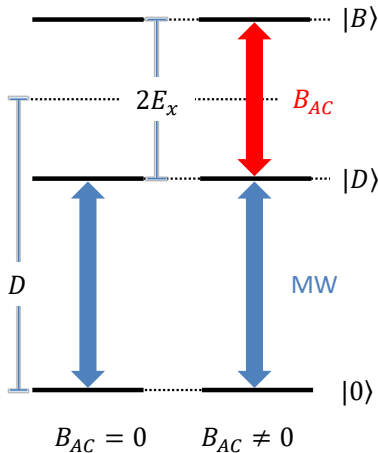


FIG. 1. Energy level diagram of the NV center in diamond. To drive these states, we apply both a GHz frequency microwave field and a MHz frequency AC magnetic field.

driving microwave field (target AC magnetic field). We assume that ω_{mw} is in the order of GHz, whereas ω_{AC} is in the order of MHz. In a rotating frame defined by U , the effective Hamiltonian becomes $H' = UH U^\dagger - iU \frac{d}{dt} U^\dagger$. By considering $U = e^{i\omega_{\text{mw}} t \hat{S}_z^2}$ and using the rotating wave approximation, we obtain the following Hamiltonian.

$$H \simeq (D - \omega_{\text{mw}}) \hat{S}_z^2 + E_x (\hat{S}_x^2 - \hat{S}_y^2) + \frac{\gamma_e B_{\text{mw}}^{(x)}}{2} \hat{S}_x + \frac{\gamma_e B_{\text{mw}}^{(y)}}{2} \hat{S}_y + \gamma_e B_{\text{AC}}^{(z)} \hat{S}_z \cos(\omega_{\text{AC}} t) \quad (3)$$

$$= (D + E_x - \omega_{\text{mw}}) |B\rangle\langle B| + (D - E_x - \omega_{\text{mw}}) |D\rangle\langle D| + \frac{\gamma_e B_{\text{mw}}^{(x)}}{2} (|B\rangle\langle 0| + |0\rangle\langle B|) - \frac{i\gamma_e B_{\text{mw}}^{(y)}}{2} (|D\rangle\langle 0| - |0\rangle\langle D|) + \gamma_e B_{\text{AC}}^{(z)} (|B\rangle\langle D| + |D\rangle\langle B|) \cos(\omega_{\text{AC}} t) \quad (4)$$

In a different rotating frame defined by $U' = e^{i\frac{\omega_{\text{AC}}}{2} (\hat{S}_x^2 - \hat{S}_y^2)}$, we obtain the following Hamiltonian.

$$H = \left(D + E_x - \omega_{\text{mw}} - \frac{1}{2} \omega_{\text{AC}} \right) |B\rangle\langle B| + \left(D - E_x - \omega_{\text{mw}} + \frac{1}{2} \omega_{\text{AC}} \right) |D\rangle\langle D| + \frac{\gamma_e B_{\text{mw}}^{(x)}}{2} \left(e^{i\frac{\omega_{\text{AC}} t}{2}} |B\rangle\langle 0| + e^{-i\frac{\omega_{\text{AC}} t}{2}} |0\rangle\langle B| \right) - \frac{i\gamma_e B_{\text{mw}}^{(y)}}{2} \left(e^{-i\frac{\omega_{\text{AC}} t}{2}} |D\rangle\langle 0| - e^{i\frac{\omega_{\text{AC}} t}{2}} |0\rangle\langle D| \right) + \frac{1}{2} \gamma_e B_{\text{AC}}^{(z)} (|B\rangle\langle D| + |D\rangle\langle B|) \quad (5)$$

where we have again used the rotating wave approximation.

Importantly, an AC magnetic field in the z direction [the fifth term in the Hamiltonian (5)] induces the transition between $|B\rangle$ and $|D\rangle$ when the frequency of the field is in resonance with the energy difference between $|B\rangle$ and $|D\rangle$. Without the AC magnetic field, we can only induce transitions between the ground state $|0\rangle$ and the bright (dark) state $|B\rangle$ [$|D\rangle$] via the microwave radiation with a frequency of $\omega_{\text{mw}} \simeq D + E_x$ ($\omega_{\text{mw}} \simeq D - E_x$) in the conventional CW-ODMR setup. $|B\rangle$ and $|D\rangle$ the applied AC magnetic field and the microwave field can drive transitions from the ground state to the bright and dark states. Thus, the results of CW-ODMR with an applied AC magnetic field should differ from those of CW-ODMR without any AC magnetic field.

We now quantify the change in the CW-ODMR signal that occurs because of the AC magnetic fields first focusing on the transition induced between $|B\rangle$ and $|D\rangle$ by the AC magnetic field with a frequency of $\omega_{\text{AC}} = 2E_x$. We assume a weak amplitude for the AC magnetic field so that we can use time dependent perturbation theory. In

the interaction picture, we obtain

$$\begin{aligned}
H_I = & \frac{\gamma_e B_{\text{mw}}^{(x)}}{2\sqrt{2}} e^{i(D-\omega_{\text{mw}} + \frac{\gamma_e B_{\text{AC}}^{(z)}}{2} + E_x)t} |1\rangle\langle 0| \\
& + e^{i(D-\omega_{\text{mw}} - \frac{\gamma_e B_{\text{AC}}^{(z)}}{2} + E_x)t} |-1\rangle\langle 0| + \text{hc} \\
& - \frac{i\gamma_e B_{\text{mw}}^{(y)}}{2\sqrt{2}} (e^{i(D-\omega_{\text{mw}} + \frac{\gamma_e B_{\text{AC}}^{(z)}}{2} - E_x)t} |1\rangle\langle 0| \\
& - e^{i(D-\omega_{\text{mw}} - \frac{\gamma_e B_{\text{AC}}^{(z)}}{2} - E_x)t} |-1\rangle\langle 0| + \text{hc}) \quad (6)
\end{aligned}$$

By using Fermi's golden rule, we can show that the transition from the ground state to the higher energy eigenstates $\omega_{\text{mw}} \simeq D \pm \gamma_e B_{\text{AC}}^{(z)}/2 \pm E_x$ (Fig. 1). Thus, applying an external AC magnetic field changes the dip structure in CW-ODMR.

We now describe the details of the diamond sample used in our experiment. We used an ensemble of NV centers in a diamond film on a (001) electronic grade substrate. The isotopically purified ^{12}C diamond film ($[^{12}\text{C}] = 99.999\%$) was grown using nitrogen doped microwave plasma assisted chemical vapor deposition. To both increase the NV center density and improve the coherence time²⁴, the sample was irradiated with ion doses of 10^{12} cm^{-3} with 15 keV He^+ ions and was annealed for 24 h in vacuum at 800 °C. The NV density was estimated to be of the order of 10^{15} cm^{-3} .

Now, we explain the experiment of sensing an AC magnetic field using CW-ODMR. For these experiments, we used a homebuilt system for confocal laser scanning microscopy with a spatial resolution of 400 nm. The diamond sample was positioned above the antenna²⁵ used to emit the microwave radiation. A 30 μm diameter copper wire is placed in contact with the sample surface to apply the target AC magnetic field, which is detected by measuring the difference in the CW-ODMR spectrum.

Figure 2 shows the signal from the conventional CW-ODMR technique (with no external AC magnetic field); the resonance frequency is split by about 4 MHz because of a local magnetic field and strain from impurities in diamond^{22,23}. This splitting gives the energy difference between $|B\rangle$ and $|D\rangle$. ODMR is performed by applying an AC magnetic field with a frequency of $f_{\text{AC}} = \omega_{\text{AC}}/2\pi = 4 \text{ MHz}$ and a magnetic field amplitude $B_{\text{AC}} = 7.7 \mu\text{T}$ to induce transitions between $|B\rangle$ and $|D\rangle$. The result in Fig. 2 shows the difference in the spectrum due to the external AC magnetic field, and it demonstrates the detection of the external AC magnetic fields by CW-ODMR.

Since we use the resonance between $|B\rangle$ and $|D\rangle$, the frequency band in which AC magnetic fields may be detected is determined by the width of the split in the CW-ODMR spectrum.

As noted in Eq. (5), this splitting may be increased by applying an electric field²⁶, which provides a way to determine which frequency of the AC magnetic field will be detected. Straightforward calculations show that the detectable frequencies range from hundreds of kHz to hundreds of MHz. The lower limit is determined by the

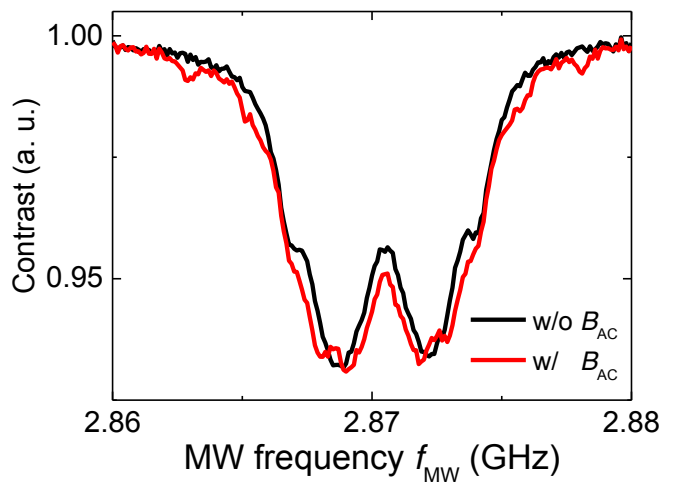


FIG. 2. ODMR with and without an AC magnetic field ($B_{\text{AC}} \cos 2\pi f_{\text{AC}}$) for $B_{\text{AC}} = 7.7 \mu\text{T}$ and $f_{\text{AC}} = 4 \text{ MHz}$. Here, no DC magnetic field is applied. The application of an AC magnetic field changes the ODMR spectrum.

resonance linewidth of the ODMR spectrum with 200 kHz currently being the minimum linewidth²⁴. However, the upper limit is determined by the breakdown field in diamond. The splitting width due to the Stark effect is given as $2RE_x$, so the maximum splitting width is 340 MHz because the Stark shift constant $R = 17 \text{ Hz cm/V}^{27}$ and the breakdown electric field of diamond $E = 10 \text{ MV/m}^{28}$.

Next, we measure ODMR dependence on the amplitude of the AC magnetic field. The ODMR spectrum with various AC magnetic field amplitudes is shown in Fig. 3 where we set $f_{\text{AC}} = 4 \text{ MHz}$. While two resonances are observed without applying the AC magnetic fields, the resonance is split into four lines, and the split becomes larger as we increase the amplitude of the AC magnetic

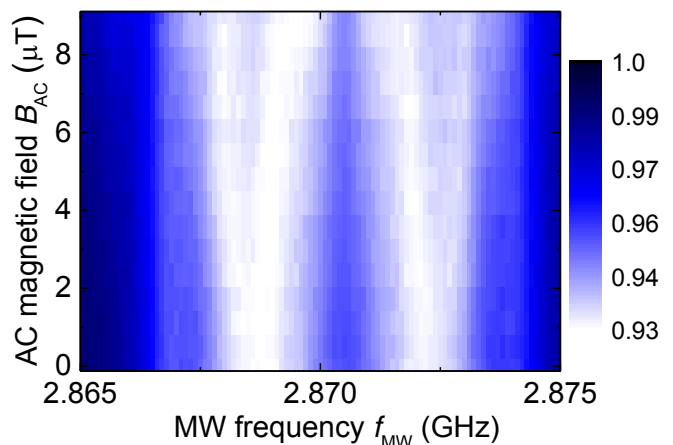


FIG. 3. ODMR spectrum with applied AC magnetic fields. Here, the x and y axes denote the frequency of the microwave and the amplitude of the AC magnetic fields, respectively. Four resonances are observed with the applied AC magnetic fields.

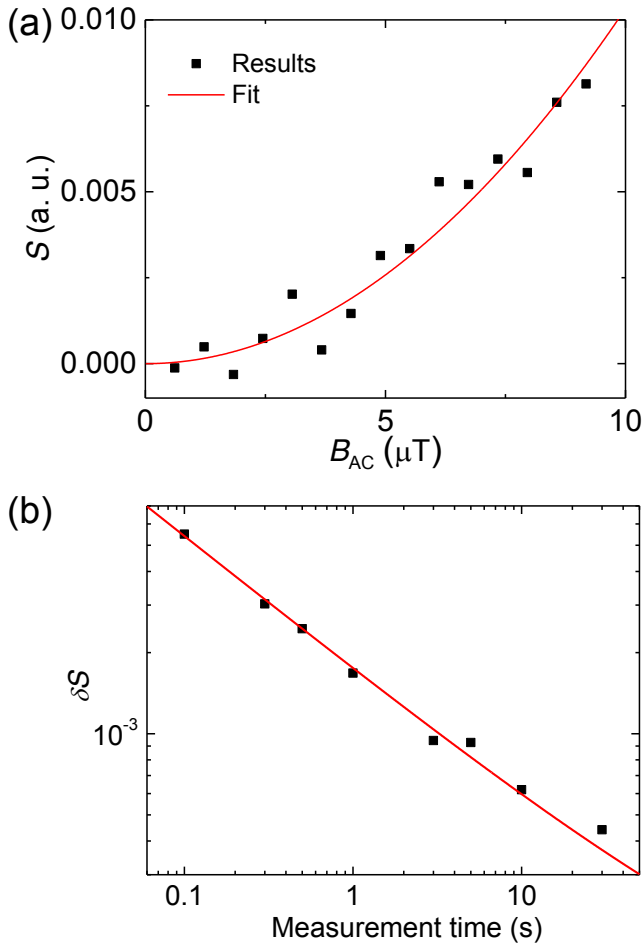


FIG. 4. Measured signal and standard deviation of the ODMR signal. (a) ODMR signal plotted against the amplitude of the AC magnetic field. The data are fit to the function $S - S_0 = a(B_{AC})^2$, where a is a fitting parameter and S_0 is the offset. The fit shows that the signal is quadratic in the amplitude of the AC magnetic field. (b) Standard deviation δS of the ODMR signal as a function of measurement time.

fields. This is consistent with our derived formula that represents the resonance $\omega_{mw} \simeq D \pm \gamma_e B_{AC}^{(z)}/2 \pm E_x$.

In Fig. 4(a), we plot the ODMR signal against the amplitude of the AC magnetic field, with the microwave frequency $f_{mw} = \omega_{mw}/2\pi = 2.86887$ GHz, which is one of the two resonance frequencies obtained with no external AC magnetic field. The signal quadratically depends on the amplitude, which can be quantitatively understood as follows. We represent the two resonances around $D - E_x$ as the sum of two Lorentzian functions: $F(B) = \sum_{j=\pm 1} 1/((f_{mw} - (D + j\gamma_e B_{AC}^{(z)}/2 - E_x))^2 + \gamma^2)$, where γ is the linewidth. In this case, we obtain $dF(B)/dB \propto B$ for small B , which this shows the quadratic dependence.

To estimate the magnetic sensitivity δB_{AC} from the experimental results, we must determine the signal fluctuation δS where S corresponds to the photoluminescence in ODMR³. As shown in Fig. 4(b), the fluctuation decreases with the relation \sqrt{T} , where T is the mea-

surement time. From these experimental observations, we estimate the sensitivity of the method for detecting AC magnetic fields to be $2.5 \mu\text{T}/\sqrt{\text{Hz}}$. Note that the sensitivity could be improved by using a NV center in diamond with a narrow linewidth²⁴ and with an almost perfect preferential orientation of the axis²⁹⁻³¹ and a high density of the NV centers^{24,31,32}. In fact, by using the parameters reported in³¹, we estimate that the proposed method would have a sensitivity of $50 \text{ nT}/\sqrt{\text{Hz}}$.

In conclusion, we report a method to detect MHz frequency AC magnetic fields that uses CW-ODMR by exploiting NV centers in diamond. By simply applying a continuous microwave field and optical laser irradiation, the method provides a sensitivity of $2.5 \mu\text{T}/\sqrt{\text{Hz}}$ at room temperature. The experimental setup is very simple because it requires neither an external DC magnetic field nor a pulse sequence. These results pave the way to realize a practical and feasible AC magnetic field sensor.

We thank H. Toida and K. Kakuyanagi for helpful discussions. This work was supported by JSPS KAKENHI Grant No. 15K17732. This work was also supported by MEXT KAKENHI Grants No. 15H05868, No. 15H05870, No. 15H03996, No. 26220602, and No. 26249108. This work was also supported by the Advanced Photon Science Alliance (APSA), JSPS Core-to-Core Program FY2013 Projects No.2, and Spin-NRJ.

- ¹T. Wolf, P. Neumann, K. Nakamura, H. Sumiya, T. Ohshima, J. Isoya, and J. Wrachtrup, *Phys. Rev. X* **5**, 041001 (2015).
- ²G. Balasubramanian, I. Y. Chan, R. Kolesov, M. Al-Hmoud, J. Tisler, C. Shin, C. Kim, A. Wojcik, P. R. Hemmer, A. Krueger, T. Hanke, A. Leitenstorfer, R. Bratschitsch, F. Jelezko, and J. Wrachtrup, *Nature* **455**, 648 (2008).
- ³J. M. Taylor, P. Cappellaro, L. Childress, L. Jiang, D. Budker, P. R. Hemmer, A. Yacoby, R. Walsworth, and M. D. Lukin, *Nat. Phys.* **4**, 810 (2008).
- ⁴B. J. Maertz, A. P. Wijnheijmer, G. D. Fuchs, M. E. Nowakowski, and D. D. Awschalom, *Appl. Phys. Lett.* **96**, 092504 (2010).
- ⁵R. S. Schoenfeld and W. Harneit, *Phys. Rev. Lett.* **106**, 030802 (2011).
- ⁶L. M. Pham, D. Le Sage, P. L. Stanwix, T. K. Yeung, D. Glenn, A. Trifonov, P. Cappellaro, P. R. Hemmer, M. D. Lukin, H. Park, A. Yacoby, and R. L. Walsworth, *New J. Phys.* **13**, 045021 (2011).
- ⁷D. Le Sage, K. Arai, D. R. Glenn, S. J. Devience, L. M. Pham, L. Rahn-Lee, M. D. Lukin, A. Yacoby, A. Komeili, and R. L. Walsworth, *Nature* **496**, 486 (2013).
- ⁸S. Steinert, F. Ziem, L. T. Hall, A. Zappe, M. Schweikert, N. Götz, A. Aird, G. Balasubramanian, L. Hollenberg, and J. Wrachtrup, *Nat. Commun.* **4**, 1607 (2013).
- ⁹S. J. Devience, L. M. Pham, I. Lovchinsky, A. O. Sushkov, N. Bar-Gill, C. Belthangady, F. Casola, M. Corbett, H. Zhang, M. Lukin, H. Park, A. Yacoby, and R. L. Walsworth, *Nat. Nanotechnol.* **10**, 129 (2015).
- ¹⁰D. R. Glenn, K. Lee, H. Park, R. Weissleder, A. Yacoby, M. D. Lukin, H. Lee, R. L. Walsworth, and C. B. Connolly, *Nat. Methods* **12**, 736 (2015).
- ¹¹P. Maletinsky, S. Hong, M. S. Grinolds, B. Hausmann, M. D. Lukin, R. L. Walsworth, M. Loncar, and A. Yacoby, *Nat. Nanotechnol.* **7**, 320 (2012).
- ¹²L. Rondin, J. P. Tetienne, P. Spinicelli, C. Dal Savio, K. Karrai, G. Dantelle, A. Thiaville, S. Rohart, J. F. Roch, and V. Jacques, *Appl. Phys. Lett.* **100**, 153118 (2012).
- ¹³J.-P. Tetienne, T. Hingant, J.-V. Kim, L. H. Diez, J.-P. Adam, K. Garcia, J.-F. Roch, S. Rohart, A. Thiaville, D. Ravelosona, and V. Jacques, *Science* **344**, 1366 (2014).
- ¹⁴P. Appel, E. Neu, M. Ganzhorn, A. Barfuss, M. Batzer, M. Gratz, A. Tschöpe, and P. Maletinsky, *Rev. Sci. Instrum.* **87**, 063703 (2016).

- ¹⁵K. Chang, A. Eichler, J. Rhensius, L. Lorenzelli, and C. L. Degen, *Nano Lett.* **17**, 2367 (2017).
- ¹⁶C. L. Degen, *Appl. Phys. Lett.* **92**, 243111 (2008).
- ¹⁷J. R. Maze, P. L. Stanwix, J. S. Hodges, S. Hong, J. M. Taylor, P. Cappellaro, L. Jiang, M. V. G. Dutt, E. Togan, A. S. Zibrov, A. Yacoby, R. L. Walsworth, and M. D. Lukin, *Nature* **455**, 644 (2008).
- ¹⁸K. Jensen, N. Leefer, A. Jarmola, Y. Dumeige, V. M. Acosta, P. Kehayias, B. Patton, and D. Budker, *Phys. Rev. Lett.* **112**, 160802 (2014).
- ¹⁹S. Ahmadi, H. A. El-Ella, J. O. Hansen, A. Huck, and U. L. Andersen, *Phys. Rev. Appl.* **8**, 034001 (2017).
- ²⁰T. Tashima, H. Morishita, and N. Mizuochi, (2017), arXiv:1712.04615.
- ²¹K. Fang, V. M. Acosta, C. Santori, Z. Huang, K. M. Itoh, H. Watanabe, S. Shikata, and R. G. Beausoleil, *Phys. Rev. Lett.* **110**, 130802 (2013).
- ²²X. Zhu, Y. Matsuzaki, R. Amsüss, K. Kakuyanagi, T. Shimo-Oka, N. Mizuochi, K. Nemoto, K. Semba, W. J. Munro, and S. Saito, *Nat. Commun.* **5**, 3424 (2014).
- ²³Y. Matsuzaki, H. Morishita, T. Shimooka, T. Tashima, K. Kakuyanagi, K. Semba, W. J. Munro, H. Yamaguchi, N. Mizuochi, and S. Saito, *J. Phys. Condens. Matter* **28**, 275302 (2016).
- ²⁴E. E. Kleinsasser, M. M. Stanfield, J. K. Q. Banks, Z. Zhu, W.-D. Li, V. M. Acosta, H. Watanabe, K. M. Itoh, and K.-M. C. Fu, *Appl. Phys. Lett.* **108**, 202401 (2016).
- ²⁵K. Sasaki, E. E. Kleinsasser, Z. Zhu, W. D. Li, H. Watanabe, K. M. C. Fu, K. M. Itoh, and E. Abe, *Appl. Phys. Lett.* **110**, 192407 (2017).
- ²⁶T. Iwasaki, W. Naruki, K. Tahara, T. Makino, H. Kato, M. Ogura, D. Takeuchi, S. Yamasaki, and M. Hatano, *ACS Nano* **11**, 1238 (2017).
- ²⁷E. Van Oort and M. Glasbeek, *Chem. Phys. Lett.* **168**, 529 (1990).
- ²⁸A. T. Collins, *Properties and Growth of Diamond*, edited by G. Davies (Inspec, 1994).
- ²⁹J. Michl, T. Teraji, S. Zaiser, I. Jakobi, G. Waldherr, F. Dolde, P. Neumann, M. W. Doherty, N. B. Manson, J. Isoya, and J. Wrachtrup, *Appl. Phys. Lett.* **104**, 102407 (2014).
- ³⁰T. Fukui, Y. null, T. Miyazaki, Y. Miyamoto, H. Kato, T. Matsumoto, T. Makino, S. Yamasaki, R. Morimoto, N. Tokuda, M. Hatano, Y. Sakagawa, H. Morishita, T. Tashima, S. Miwa, Y. Suzuki, and N. Mizuochi, *Appl. Phys. Express* **7**, 055201 (2014).
- ³¹H. Ozawa, K. Tahara, H. Ishiwata, M. Hatano, and T. Iwasaki, *Appl. Phys. Express* **10**, 045501 (2017).
- ³²V. M. Acosta, E. Bauch, M. P. Ledbetter, C. Santori, K.-M. C. Fu, P. E. Barclay, R. G. Beausoleil, H. Linget, J. F. Roch, F. Treussart, S. Chemerisov, W. Gawlik, and D. Budker, *Phys. Rev. B* **80**, 115202 (2009).